

Article

Regulation of Epithelial–Mesenchymal Transition Pathway and Artificial Intelligence-Based Modeling for Pathway Activity Prediction

Shihori Tanabe ^{1,*} , Sabina Quader ² , Ryuichi Ono ³, Horacio Cabral ⁴, Kazuhiko Aoyagi ⁵, Akihiko Hirose ¹, Edward J. Perkins ⁶, Hiroshi Yokozaki ⁷  and Hiroki Sasaki ⁸

¹ Division of Risk Assessment, Center for Biological Safety and Research, National Institute of Health Sciences, Kawasaki 210-9501, Japan

² Innovation Center of NanoMedicine (iCONM), Kawasaki Institute of Industrial Promotion, Kawasaki 210-0821, Japan

³ Division of Cellular and Molecular Toxicology, Center for Biological Safety and Research, National Institute of Health Sciences, Kawasaki 210-9501, Japan

⁴ Department of Bioengineering, Graduate School of Engineering, The University of Tokyo, Tokyo 113-0033, Japan

⁵ Department of Clinical Genomics, National Cancer Center Research Institute, Tokyo 104-0045, Japan

⁶ Environmental Laboratory, US Army Engineer Research and Development Center, Vicksburg, MS 39180, USA

⁷ Department of Pathology, Kobe University of Graduate School of Medicine, Kobe 650-0017, Japan

⁸ Department of Translational Oncology, National Cancer Center Research Institute, Tokyo 104-0045, Japan

* Correspondence: stanabe@nihs.go.jp; Tel.: +81-44-270-6686

Simple Summary: Molecular network pathways are activated or inactivated under various conditions. Previously, we revealed that epithelial–mesenchymal transition (EMT) is a feature of diffuse-type gastric cancer. Here, we modeled the activation states of EMT in the development pathway using molecular pathway images and artificial intelligence (AI). The regulation of EMT in the development pathway was activated in diffuse-type gastric cancer (GC) and inactivated in intestinal-type GC. AI modeling with molecular pathway images generated a highly accurate Elastic-Net Classifier models that was validated with 10 additional activated and 10 inactivated pathway images.

Abstract: Because activity of the epithelial–mesenchymal transition (EMT) is involved in anti-cancer drug resistance, cancer malignancy, and shares some characteristics with cancer stem cells (CSCs), we used artificial intelligence (AI) modeling to identify the cancer-related activity of the EMT-related pathway in datasets of gene expression. We generated images of gene expression overlaid onto molecular pathways with Ingenuity Pathway Analysis (IPA). A dataset of 50 activated and 50 inactivated pathway images of EMT regulation in the development pathway was then modeled by the DataRobot Automated Machine Learning platform. The most accurate models were based on the Elastic-Net Classifier algorithm. The model was validated with 10 additional activated and 10 additional inactivated pathway images. The generated models had false-positive and false-negative results. These images had significant features of opposite labels, and the original data were related to Parkinson’s disease. This approach reliably identified cancer phenotypes and treatments where EMT regulation in the development pathway was activated or inactivated thereby identifying conditions where therapeutics might be applied or developed. As there are a wide variety of cancer phenotypes and CSC targets that provide novel insights into the mechanism of CSCs’ drug resistance and cancer metastasis, our approach holds promise for modeling and simulating cellular phenotype transition, as well as predicting molecular-induced responses.

Keywords: artificial intelligence; epithelial–mesenchymal transition; Ingenuity Pathway Analysis; machine learning; molecular pathway network



Citation: Tanabe, S.; Quader, S.; Ono, R.; Cabral, H.; Aoyagi, K.; Hirose, A.; Perkins, E.J.; Yokozaki, H.; Sasaki, H. Regulation of Epithelial–Mesenchymal Transition Pathway and Artificial Intelligence-Based Modeling for Pathway Activity Prediction. *Onco* **2023**, *3*, 13–25. <https://doi.org/10.3390/onco3010002>

Academic Editor: Galatea Kallergi

Received: 17 November 2022

Revised: 29 December 2022

Accepted: 3 January 2023

Published: 6 January 2023



Copyright: © 2023 by the authors. Licensee MDPI, Basel, Switzerland. This article is an open access article distributed under the terms and conditions of the Creative Commons Attribution (CC BY) license (<https://creativecommons.org/licenses/by/4.0/>).

1. Introduction

Molecular network pathways are activated or inactivated under many different conditions. Previously, we found that diffuse-type gastric cancer (GC) has a feature of epithelial-mesenchymal transition (EMT) [1–3]. EMT is involved in anti-cancer drug resistance, cancer malignancy, metastasis, and cancer stem cells (CSCs) [4–7]. Experiments in anti-cancer drug-resistant cancer cell lines indicate that EMT is involved in cancer cell drug resistance [8], highlighting the significance of EMT targeting in cancer treatment [6].

Several signaling pathways involved in EMT contribute to drug resistance [6]. Tumor growth factor beta (TGF β) signaling activates SMAD2/3, which then complexes with SMAD4 to form a trimetric SMAD complex, leading to the transcription of EMT transcription factors [9]. Wnt/ β -catenin signaling activates Snail transcription to induce EMT [6,10]. Recent studies have also revealed the role of EMT in autophagy and CSCs during metastasis [11,12]. However, the relationship between the EMT pathway activation state and therapeutic responsiveness is not fully understood.

Understanding the activity state of the EMT pathway in cancer cells may be an important clue for identifying therapeutic targets in malignant cancers. To effectively predict EMT activity and potential therapeutic responsiveness, molecular pathway images were used to capture activity of EMT-related pathways of datasets in Ingenuity Pathway Analysis (IPA), followed by artificial intelligence (AI) modeling with images of gene expression activity in the pathway.

2. Materials and Methods

2.1. Data Analysis of Diffuse- and Intestinal-Type GC

We used RNA sequencing data of diffuse- and intestinal-type GC, which are publicly available in The Cancer Genome Atlas (TCGA) of the cBioPortal for Cancer Genomics database at the National Cancer Institute (NCI) Genomic Data Commons (GDC) data portal [13–17]. Publicly available data on stomach adenocarcinoma in the TCGA, Stomach Adenocarcinoma (TCGA, PanCancer Atlas), [13–16] were compared between diffuse-type GC, which is genomically stable ($n = 50$), and intestinal GC, which has a feature of chromosomal instability ($n = 223$), in TCGA Research Network publications, as previously described [1,14,18].

2.2. Network Analysis

Data on intestinal- and diffuse-type GC from the TCGA cBioPortal for Cancer Genomics were uploaded and analyzed using IPA (Qiagen, CA, USA) [19,20]. The datasets of gene expression in diseases were searched in IPA, and datasets with absolute values in z-score in the top 60 for activated state and inactivated state (total of 120) in regulation of EMT in the development pathway were extracted for AI prediction modeling and evaluation. Among 120 analyses in the activity plot of regulation of EMT in the development pathway, 50 activated and 50 inactivated analyses (total of 100) were used to generate AI models and 10 activated and 10 inactivated analyses (total of 20) were withheld for use in validating the generated model. The 100 analyses (50 activated and 50 inactivated states) found in the database of IPA and newly used to generate AI-based models are summarized in Table 1.

Table 1. Analyses in the regulation of EMT in the development pathway for AI prediction modeling.

Analysis Name	Disease State	Target Gene	Treatment	EMT
996-Breast ductal carcinoma torin 2 28190	Breast ductal carcinoma	Mtor	Torin 2	TRUE
16332-Fibrocystic breast disease neratinib 7038	Fibrocystic breast disease	Her2; egfr	Neratinib	TRUE
16885-Fibrocystic breast disease erlotinib 7651	Fibrocystic breast disease	Egfr	Erlotinib	TRUE
116-Bone osteosarcoma (OS) MK2206 2727	Bone osteosarcoma (OS)		MK2206	TRUE
1766-Breast ductal carcinoma brivanib 8512	Breast ductal carcinoma	Vegfr; fgfr	Brivanib	TRUE
47-Huntington's disease (HD) haloperidol 12804	Huntington's disease (HD)		Haloperidol	TRUE
4874-Melanoma crizotinib 22540	Melanoma	Alk and ros1	Crizotinib	TRUE
6785-Non-small cell lung carcinoma ZSTK474 24663	Non-small cell lung carcinoma	PI3K	ZSTK474	TRUE
7-Normal control differentiation medium 10230	Normal control		Differentiation medium	TRUE
13972-Prostate adenocarcinoma (PRAD) PI103 4415	Prostate adenocarcinoma (PRAD)	PI3K	PI103	TRUE
16046-Prostate adenocarcinoma (PRAD) MK2206 6720	Prostate adenocarcinoma (PRAD)	AKT	MK2206	TRUE
7063-Breast adenocarcinoma linifanib 24973	Breast adenocarcinoma	Rtk; vegf; pdgf	Linifanib	TRUE
7923-Breast adenocarcinoma PF3758309 25928	Breast adenocarcinoma	PAK4	PF3758309	TRUE
2-Breast carcinoma beta-estradiol (E2) 3915	Breast carcinoma		B-estradiol (E2)	TRUE
10974-Breast ductal carcinoma KIN001-043 1084	Breast ductal carcinoma	GSK3 β	KIN001-043	TRUE
1116-Breast ductal carcinoma QL-X-138 1291	Breast ductal carcinoma	BTK; MNK	QL-X-138	TRUE
29-Colon cancer GSK525762A; trametinib 3009	Colon cancer		GSK525762A; trametinib	TRUE
35-Colon cancer active JQ1 1658	Colon cancer		Active JQ1	TRUE
13176-Colorectal adenocarcinoma BGJ398 3531	Colorectal adenocarcinoma	FGFR	BGJ398	TRUE
12948-Colorectal adenocarcinoma AZ628 3277	Colorectal adenocarcinoma	BRAF; BRAFV600E; C-RAF-1	AZ628	TRUE
12715-Colorectal adenocarcinoma AT7519 3019	Colorectal adenocarcinoma	CDK	AT7519	TRUE
6-Disease control IL-1 beta 15814	Disease control		IL-1 β	TRUE
17104-Fibrocystic breast disease canertinib 7896	Fibrocystic breast disease	Egfr; her2; erbb4	Canertinib	TRUE
17239-Fibrocystic breast disease torin 1 8045	Fibrocystic breast disease	Mtor	Torin 1	TRUE
16449-Fibrocystic breast disease AZD8330 7167	Fibrocystic breast disease	MEK	AZD8330	TRUE
17590-Fibrocystic breast disease mitoxantrone 8435	Fibrocystic breast disease	Topoisomerase	Mitoxantrone	TRUE
7-Fibrosis DMSO 7394	Fibrosis		DMSO	TRUE
20894-Hepatocellular carcinoma (LIHC) chelerythrine chloride 12106	Hepatocellular carcinoma (LIHC)	PKC	Chelerythrine chloride	TRUE
59-Huntington's disease (HD) nortriptyline 12817	Huntington's disease (HD)		Nortriptyline	TRUE
2-Lung adenocarcinoma (LUAD) Transfection_HOXC6 631	Lung adenocarcinoma (LUAD)		Transfection_HOXC6	TRUE
3-Major depressive disorder differentiation medium 3130	Major depressive disorder		Differentiation medium	TRUE
5612-Melanoma AT7867 23361	Melanoma	AKT1/2/3; p70s6k/PKA	AT7867	TRUE
5173-Melanoma lapatinib 22873	Melanoma	Her2; egfr	Lapatinib	TRUE
91-Non-small cell lung carcinoma BGT226 27235	Non-small cell lung carcinoma	PI3K; mtor	BGT226	TRUE
14456-Normal control WYE125132 4953	Normal control	Mtor	WYE125132	TRUE
28175-Normal control glesatinib 20196	Normal control	C-met; tek; vegfr; ron	Glesatinib	TRUE
60-Normal control 567	Normal control			TRUE
2-Normal control culture medium 1187	Normal control		Culture medium	TRUE

Table 1. Cont.

Analysis Name	Disease State	Target Gene	Treatment	EMT
9914-Normal control EX527 28140	Normal control	SIRT1	EX527	TRUE
4-Normal control suberoylanilide hydroxamic acid (SAHA) 2204	Normal control		Suberoylanilide hydroxamic acid (SAHA)	TRUE
27560-Normal control BMS509744 19513	Normal control	ITK	BMS509744	TRUE
14256-Normal control AZD8055 4731	Normal control	Mtor	AZD8055	TRUE
19-Normal control no serum 3447	Normal control		No serum	TRUE
5-Parkinson's disease (PD) differentiation medium 4389	Parkinson's disease (PD)		Differentiation medium	TRUE
23661-Prostate adenocarcinoma (PRAD) AZD5438 15181	Prostate adenocarcinoma (PRAD)	CDK	AZD5438	TRUE
25661-Breast adenocarcinoma omipalisib 17403	Breast adenocarcinoma	Pi3k	Omipalisib	TRUE
90-Prostate adenocarcinoma (PRAD) monolayer culture 4346	Prostate adenocarcinoma (PRAD)		Monolayer culture	TRUE
8-Normal control lipopolysaccharide (LPS) 4907	Normal control		Lipopolysaccharide (LPS)	TRUE
2-Acute myeloid leukemia (LAML) lipopolysaccharide (LPS) 9357	Acute myeloid leukemia (LAML)		Lipopolysaccharide (LPS)	TRUE
25084-Breast adenocarcinoma CGP60474 16762	Breast adenocarcinoma	CDK1; CDK2	CGP60474	TRUE
20-Non-small cell lung carcinoma IFN gamma 13421	Non-small cell lung carcinoma		Ifn γ	FALSE
7-Normal control co-culture 3087	Normal control		Co-culture	FALSE
5-Normal control hypoxia 13911	Normal control		Hypoxia	FALSE
1-Normal control IFN alpha 4636	Normal control		Ifn α	FALSE
11-Normal control differentiation medium 10205	Normal control		Differentiation medium	FALSE
3-Normal control Infection_human betaherpesvirus 5 (HHV5) 15858	Normal control		Infection_human betaherpesvirus 5 (HHV5)	FALSE
31-Bone osteosarcoma (OS) 1,9-pyrazoloanthrone 2804	Bone osteosarcoma (OS)		1,9-pyrazoloanthrone	FALSE
57-Coronavirus disease 2019 (COVID-19) 96	Coronavirus disease 2019 (COVID-19)			FALSE
17503-Fibrocystic breast disease HG6-64-1 8339	Fibrocystic breast disease	B-RAF	HG6-64-1	FALSE
11-Genetic disease 444	Genetic disease			FALSE
4-Glioblastoma (GBM) differentiation medium 6303	Glioblastoma (GBM)		Differentiation medium	FALSE
23448-Hepatocellular carcinoma (LIHC) imatinib 14944	Hepatocellular carcinoma (LIHC)	BCR-ABL	Imatinib	FALSE
86-Huntington's disease (HD) sodium butyrate 12847	Huntington's disease (HD)		Sodium butyrate	FALSE
21-Mantle cell lymphoma DMSO 3032	Mantle cell lymphoma		DMSO	FALSE
5-Non-alcoholic steatohepatitis (NASH) none 11484	Non-alcoholic steatohepatitis (NASH)		None	FALSE
10431-Normal control RAF265 482	Normal control	C-RAF; B-RAF; B-RAFV600E	RAF265	FALSE
11-Normal control differentiation medium 4490	Normal control		Differentiation medium	FALSE
14744-Normal control dasatinib 5273	Normal control	Src family	Dasatinib	FALSE
65-Normal control IL-3 17225	Normal control		IL-3	FALSE
14639-Normal control saracatinib 5156	Normal control	Src; bcr-abl	Saracatinib	FALSE
3-Normal control DHA-5-HT 4554	Normal control		DHA-5-HT	FALSE

Table 1. Cont.

Analysis Name	Disease State	Target Gene	Treatment	EMT
28-Prostatic intraepithelial neoplasia (PIN) plumbagin 49	Prostatic intraepithelial neoplasia (PIN)		Plumbagin	FALSE
4-Normal control differentiation medium 3415	Normal control		Differentiation medium	FALSE
9-Huntington's disease (HD) meclizine 12851	Huntington's disease (HD)		Meclizine	FALSE
6-Normal control culture medium 593	Normal control		Culture medium	FALSE
22597-Normal control GSK429286A 13998	Normal control	ROCK1; ROCK2	GSK429286A	FALSE
8-Normal control 3-D culture; co-culture; differentiation 3017	Normal control		3D culture; co-culture; differentiation medium	FALSE
110-Normal control 109	Normal control			FALSE
26-Bone osteosarcoma (OS) nilotinib 2798	Bone osteosarcoma (OS)		Nilotinib	FALSE
26025-Breast adenocarcinoma saracatinib 17808	Breast adenocarcinoma	Src; bcr-abl	Saracatinib	FALSE
11577-Breast ductal carcinoma crizotinib 1754	Breast ductal carcinoma	Alk and ros1	Crizotinib	FALSE
17316-Fibrocystic breast disease KIN001-043 8131	Fibrocystic breast disease	GSK3 β	KIN001-043	FALSE
2-Fibrosis SB525334 7389	Fibrosis		SB525334	FALSE
52-Huntington's disease (HD) meclizine 12810	Huntington's disease (HD)		Meclizine	FALSE
1-Normal control culture medium 1186	Normal control		Culture medium	FALSE
17-Normal control differentiation medium 4496	Normal control		Differentiation medium	FALSE
6-Normal control hypoxia 13912	Normal control		Hypoxia	FALSE
2-Major depressive disorder differentiation medium 3129	Major depressive disorder		Differentiation medium	FALSE
11-Disease control none 4051	Disease control		None	FALSE
10-Normal control 3-D culture; co-culture; differentiation 2995	Normal control		3D culture; co-culture; differentiation medium	FALSE
5-Normal control lipopolysaccharide (LPS) 15704	Normal control		Lipopolysaccharide (LPS)	FALSE
1-Normal control differentiation medium 1246	Normal control		Differentiation medium	FALSE
6-Normal control 151	Normal control		3d culture; none	FALSE
10-Normal control differentiation medium 4489	Normal control		Differentiation medium	FALSE
13-Normal control co-culture 3079	Normal control		Co-culture	FALSE
13051-Colorectal adenocarcinoma BMS777607 3393	Colorectal adenocarcinoma	C-MET; AXL; RON; TYRO3	BMS777607	FALSE
27-Huntington's disease (HD) meclizine 12782	Huntington's disease (HD)		Meclizine	FALSE
8-Normal control GW3965 10098	Normal control		GW3965	FALSE
11-Normal control 368	Normal control			FALSE
6-Normal control culture medium 1191	Normal control		Culture medium	FALSE

2.3. AI Prediction Modeling

To create a prediction model using multi-modal data including images and text descriptions of molecular networks, an enterprise AI platform (DataRobot Automated Machine Learning version 7.2; DataRobot Inc. (Boston, MA, USA) was used. For the modeling, the 100 molecular networks on the regulation of EMT in the development pathway were collected and input as image data in the DataRobot (50 images in the activated state and 50 images in the inactivated state), which automatically created and tuned prediction

models using various machine-learning algorithms (e.g., eXtreme gradient-boosted trees, random forest, regularized regression such as Elastic Net, Neural Networks) [21–23]. Finally, the AI model with the highest predictive accuracy on DataRobot was identified, and various insights (such as Permutation Importance or Partial Dependence Plot) obtained from the model were reviewed. To calculate the accuracy of the model, 20 additional image data (10 images in the activated state and 10 images in the inactivated state) that were not used as training data for the AI model creation were added for validation.

2.4. Statistical Analysis

The RNA sequencing data on diffuse- and intestinal-type GC was analyzed via Student’s *t*-test. The *z*-scores of intestinal- and diffuse-type GC samples were compared, and the difference was considered significant at $p < 0.00001$, following previous reports [1,18]. The activation *z*-score in each pathway was calculated in IPA to show the level of activation.

3. Results

3.1. Regulation of the EMT in Development Pathway in Diffuse- and Intestinal-Type GC

3.1.1. Gene Expression Mapping in Regulation of the EMT in the Development Pathway in Diffuse- and Intestinal-Type GC

Alterations in gene expression in diffuse- and intestinal-type GC was mapped to a canonical pathway, “Regulation of the EMT in development pathway” (Figure 1) based on the previous gene expression analysis results [1]. Red or green color indicates upregulated or downregulated genes, respectively. In the regulation of EMT in the development pathway, frizzled and adenomatous polyposis coli regulator of the WNT signaling pathway (APC) was upregulated, while SUFU negative regulator of hedgehog signaling (SUFU), pygopus family PHD finger 2 (PYGO2), and BRCA1 was downregulated in diffuse-type GC compared to intestinal-type GC. APC encodes a tumor suppressor protein that acts as an antagonist of the Wnt signaling pathway. APC is also involved in other processes, including cell migration and adhesion, transcriptional activation, and apoptosis. SUFU is associated with β -catenin binding, protein kinase binding, and transcription regulation.

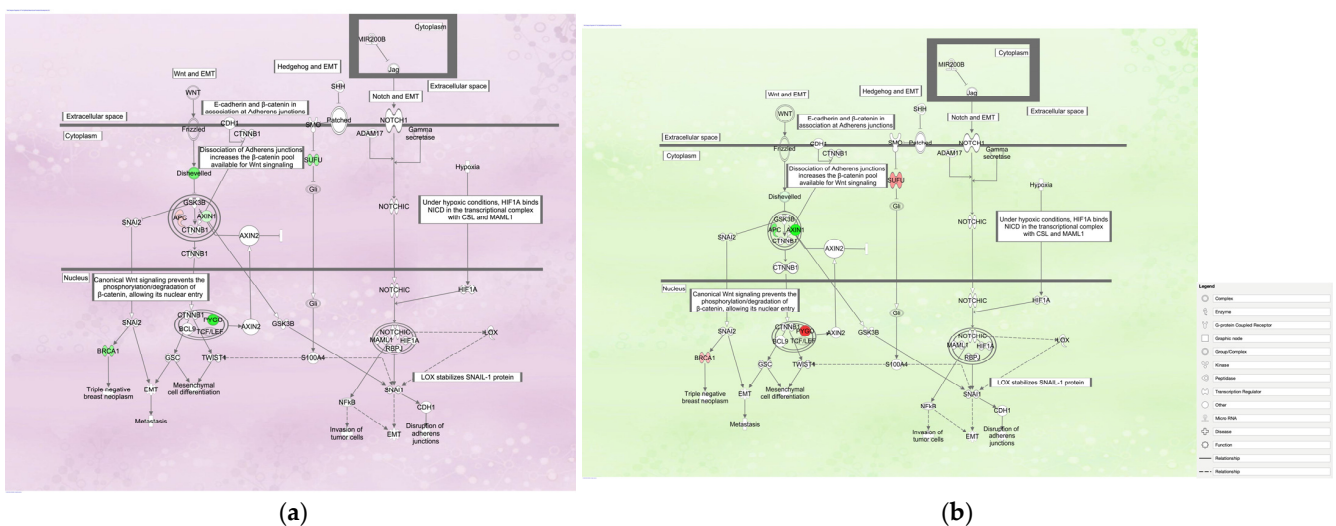


Figure 1. Regulation of the epithelial–mesenchymal transition (EMT) in development pathway in diffuse- and intestinal-type gastric cancer (GC). (a) Gene expression alteration in diffuse-type GC in regulation of the EMT in development pathway; (b) Gene expression alteration in intestinal-type GC in regulation of the EMT in development pathway. Red or green color indicates upregulated or downregulated genes, respectively. The intensity of colors indicates the degree of up- or downregulation. A solid or dashed line indicates direct or indirect interaction, respectively.

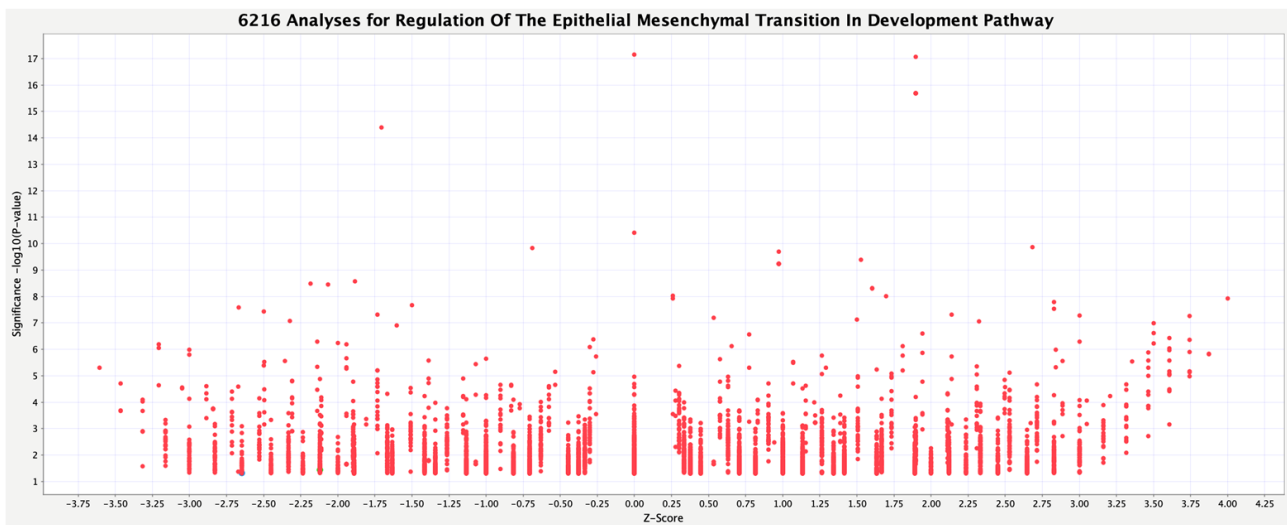


Figure 3. Activity plot of regulation of EMT in development pathway (6216 analyses, as of September 2021).

3.3. AI Modeling and Validation of the Prediction Model

The activation state of regulation of EMT in the development pathway was modeled by machine learning, including deep learning, using 50 activated and 50 inactivated images of the regulation of EMT in development pathway (Figure 4). DataRobot was used for machine-learning modeling and 34 models were automatically created, including an ElasticNet Classifier (L2/Binomial Deviance) model. DataRobot also highlighted the parts of the image data critical to the prediction accuracy of the model in an activation map (Figure 4).

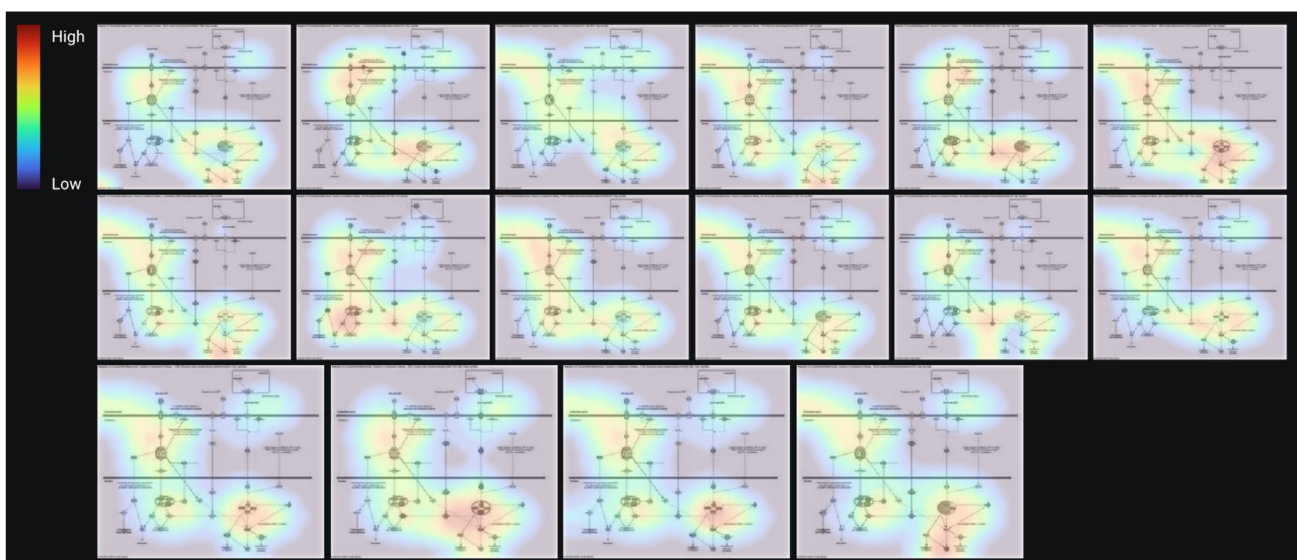


Figure 4. Activation map of AI modeling (DataRobot).

To validate the ElasticNet Classifier model, predictions were made using data on 10 activated and 10 inactivated pathway images that were not used to train the model (Table 2). The results showed that the prediction accuracy for the additional 20 images was 100% (AUC = 1.0).

Table 2. Validation of the model ElasticNet_Classifier_(L2/Binomial_Deviance).

Analysis Name	Disease State	Target Gene	Tissue	Treatment	EMT	Prediction	Label
18092-Breast adenocarcinoma CP466722 8993	breast adenocarcinoma	ATM	Breast	Cp466722	TRUE	0.9693884	1
25525-Breast adenocarcinoma celastrol 17252	breast adenocarcinoma	multiple targets	Breast	Celastrol	TRUE	0.99966132	1
25083-Breast adenocarcinoma CGP60474 16761	breast adenocarcinoma	CDK1; CDK2	Breast	Cgp60474	TRUE	0.99881416	1
18267-Breast adenocarcinoma AZD8055 9187	breast adenocarcinoma	mTOR	Breast	Azd8055	TRUE	0.99731849	1
7513-Breast adenocarcinoma OTSSP167 25473	breast adenocarcinoma	MELK	Breast	Otssp167	TRUE	0.9991679	1
18469-Breast adenocarcinoma HG6-64-1 9411	breast adenocarcinoma	B-RAF	Breast	Hg6-64-1	TRUE	0.99314697	1
25636-Breast adenocarcinoma HG6-64-1 17375	breast adenocarcinoma	B-RAF	Breast	Hg6-64-1	TRUE	0.99867832	1
14-Breast carcinoma estradiol 1431	breast carcinoma		Breast	Estradiol	TRUE	0.99207239	1
895-Breast ductal carcinoma GSK1059615 27068	breast ductal carcinoma	PI3K; mTOR	Breast	Gsk1059615	TRUE	0.98180702	1
1263-Breast ductal carcinoma lapatinib 2924	breast ductal carcinoma	HER2; EGFR	Breast	Lapatinib	TRUE	0.99916824	1
9-Normal control olive pollen extract 16317	Normal control		Peripheral blood	Olive pollen extract	FALSE	0.00276633	0
37-Normal control 257	Normal control		Lung		FALSE	0.00027655	0
21926-Normal control rebastinib 13253	Normal control	BCR-ABL	Kidney	Rebastinib	FALSE	0.08588748	0
4-Normal control mock 16535	Normal control		Bone marrow	Mock	FALSE	0.00030339	0
15884-Normal control withaferin A 6539	Normal control	IKK β	Breast	Withaferin A	FALSE	0.00271459	0

Table 2. Cont.

Analysis Name	Disease State	Target Gene	Tissue	Treatment	EMT	Prediction	Label
4-Normal control lipopolysaccharide (LPS) 15703	Normal control		Embryo	Lipopoly saccharide (LPS)	FALSE	0.00194256	0
10-Normal control co-culture 3076	Normal control		Peripheral blood	Co-culture	FALSE	0.00115878	0
6-Normal control actinomycin D 4750	Normal control		Fetal kidney	Actinomycin D	FALSE	0.01263976	0
2-Melanoma 35	Melanoma		Skin		FALSE	0.02006465	0
490-MYD88 deficiency lipopolysaccharide (LPS); polymyxin 12583	MYD88 deficiency		Peripheral blood	Lipopoly saccharide (LPS); polymyxin B	FALSE	0.03955118	0

3.4. Regulation of EMT in the Development Pathway in Other Diseases Than Cancer

The results of the modeling of regulation of EMT in the development pathway found one false-positive and one false-negative result in the model Elastic-Net Classifier in the process of the model generation (Figure 5). The analysis of the false-negative result was Parkinson’s disease with a z-score of 3 (Figure 5a). The analysis of the false-positive result was a genetic disease with a z-score of -2.646 (Figure 5b).

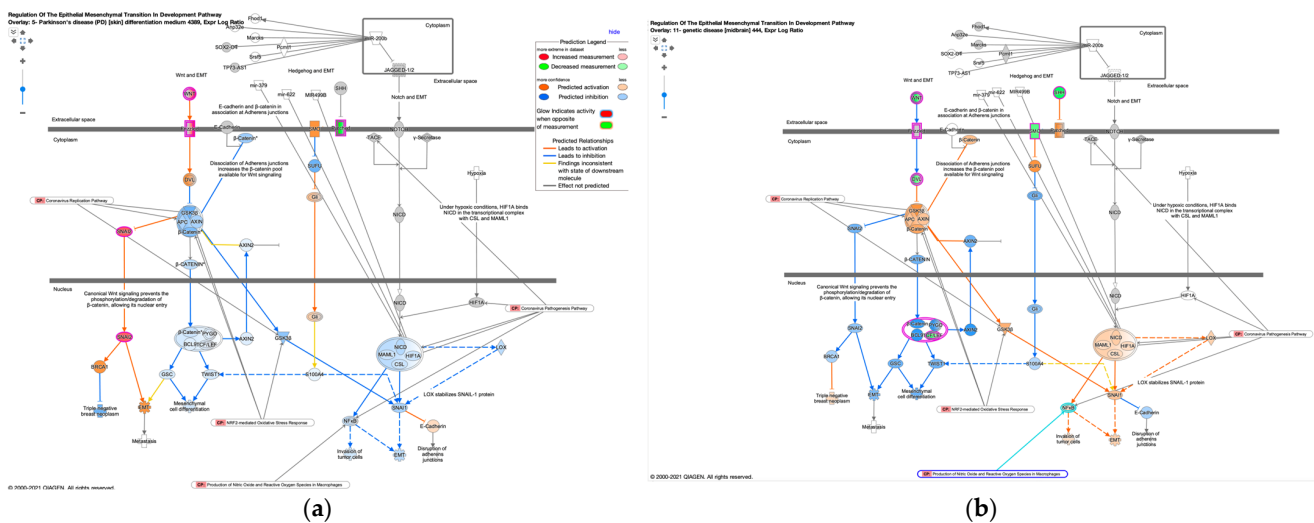


Figure 5. Regulation of EMT in development pathway in diseases. (a) Parkinson’s disease (PD) (skin) differentiation medium 4389, p value = 1.89×10^{-2} , z -score = 3; Gene identifiers marked with an asterisk (*) indicate that multiple identifiers in the dataset file map to a single gene in the Global Molecular Network. (b) genetic disease (midbrain) 444, p value = 4.75×10^{-2} , z -score = -2.646 .

4. Discussion

Our result demonstrates that the canonical pathway of regulation of the EMT in the development pathway was activated in diffuse-type GC but not in intestinal-type GC. Specifically, the pathway mapping of gene expression revealed that Frizzled and APC were upregulated, while SUFU, PYGO2, and BRCA1 were downregulated in diffuse-type GC compared to intestinal-type GC. Frizzled proteins are a family of Wnt receptors involved in carcinogenesis [24]. It was previously shown that Frizzled-7 affected stemness and chemotherapeutic resistance in GC [25]. Accordingly, targeting inhibition of Frizzled-7

attenuated spheroid formation and stemness, as well as the resistance to cisplatin, an anti-cancer drug, in GC cells may have a therapeutic effect [25]. Besides Frizzled-7, the expression of Frizzled-10 was shown to have interesting correlation with cancer evolution. Importantly, as Frizzled-10 is not expressed in fully proliferative healthy tissue, but is highly expressed in certain cancerous tissue, it has the potential to be used as a prospective receptor molecule for targeted therapy. Intriguingly, it was found that while in GC, a decrease in cytoplasmic expression of Frizzled-10 is associated with increasing malignancy, while in colon cancer, the opposite is true; increased cytoplasmic expression of Frizzled-10 is crucial for the late stages of colon cancer progression and metastasis [24]. The co-localized expression of Frizzled family in different sub-types of cancer would confer progressive features on cancer.

APC is essential as a tumor suppressor protein in colorectal cancer and for its destruction complex functions, though its specific molecular activity has not been fully resolved [26]. The modeling or simulation of the cellular phenotype transition in EMT and diseases and predicting the molecular-induced responses in diseases would be useful for future investigation.

SUFU, PYGO2, and BRCA1 were downregulated in diffuse-type GC compared to intestinal-type GC. Previous findings have reported that SUFU, a regulator of Wnt signaling, was downregulated in GC and inhibited by miRNA-324-5p [27]. It was suggested that miRNA-324-5p induces EMT by inhibiting SUFU in GC [27]. PYGO2 was reported to be increased in human breast cancer [28]. The expression of PYGO2 was also assessed in glioma tissue samples and the results showed a positive correlation between tumor grade and PYGO2 overexpression [29]. The expression of PYGO2 was overexpressed in drug-resistant cell lines of GC and GC tissue after neoadjuvant chemotherapy [30]. It may be possible that PYGO2 has a different expression profile in diffuse-type GC compared to intestinal-type GC. BRCA1 was also downregulated in diffuse-type GC compared to intestinal-type GC. We have previously shown that the role of BRCA1 in the DNA damage response pathway was activated in intestinal-type GC compared to diffuse-type GC [18]. Accordingly, BRCA1 is rather important to intestinal-type GC.

The current study successfully generated AI-based models using 50 activated and 50 inactivated images of EMT gene regulation in the development pathway. The analyses in the database were selected based on the diseases and the treatment (Tables 1 and 2). Diseases in activated states of EMT regulation in the development pathway included bone osteosarcoma [31], breast carcinoma [32], and colon cancer [33]. AI application in gastrointestinal diseases would be a promising approach [34].

An interesting point of our current study is that the machine-learning modeling revealed that an IPA analysis of Parkinson's disease had a false-negative prediction result (Figure 5a). The color of the picture seems to be inactivated, which is in accordance with the prediction result as inactivated. Furthermore, it seems that EMT activation in the WNT pathway via SNAI2 resulted in the prediction being activated, whereas CSL-HIF1A-MAML1-NICD complex-induced EMT via SNAI1 was predicted as inactivated. In addition to Parkinson's disease, the machine-learning modeling revealed that an analysis of another unrelated genetic disease had a false-positive prediction result (Figure 5b). On the other hand, based on the analysis, GSK3 β and SNAI1 were predicted as activated, while SNAI2 was inactivated (Figure 5b). The activation of GSK3 β could be associated with the mediator role of GSK3 β in the cross-talk of EMT signaling pathways [35].

5. Conclusions

The regulation of EMT in the development pathway was activated in diffuse-type GC and inactivated in intestinal-type GC. AI modeling with molecular pathway images generated the Elastic-Net Classifier model. The validation with 10 activated and 10 inactivated new pathway images, which were not used for the modeling, resulted in high accuracy. The modeling of the cellular phenotype transition in EMT and diseases will be studied in the near future.

Author Contributions: Conceptualization, S.T.; methodology, S.T.; formal analysis, S.T.; investigation, S.T.; writing—original draft preparation, S.T.; writing—review and editing, S.T., S.Q., R.O., H.C., K.A., A.H., E.J.P., H.Y. and H.S.; visualization, S.T.; project administration, S.T.; funding acquisition, S.T., S.Q., R.O. and A.H. All authors have read and agreed to the published version of the manuscript.

Funding: This research was funded by the Japan Agency for Medical Research and Development (AMED) Grant Number JP20ak0101093 (S.T., R.O. and A.H.), JP21mk0101216 (S.T.), JP22mk0101216 (S.T.), and Strategic International Collaborative Research Program, Grant Number JP20jm0210059 (S.T. and S.Q.), Japan Society for the Promotion of Science (JSPS) KAKENHI Grant Number 21K12133 (S.T. and R.O.).

Institutional Review Board Statement: Not applicable.

Informed Consent Statement: Not applicable.

Data Availability Statement: Not applicable.

Acknowledgments: The authors would like to acknowledge Shinpei Ijichi for assisting with the DataRobot Automated Machine Learning platform. The authors are grateful to all colleagues including members of the National Institute of Health Sciences, Japan for their support. This research was supported by the Ministry of Health, Labour, and Welfare, Japan.

Conflicts of Interest: The authors declare no conflict of interest.

References

1. Tanabe, S.; Quader, S.; Ono, R.; Cabral, H.; Aoyagi, K.; Hirose, A.; Yokozaki, H.; Sasaki, H. Molecular Network Profiling in Intestinal- and Diffuse-Type Gastric Cancer. *Cancers* **2020**, *12*, 3833. [[CrossRef](#)]
2. Landeros, N.; Santoro, P.M.; Carrasco-Avino, G.; Corvalan, A.H. Competing Endogenous RNA Networks in the Epithelial to Mesenchymal Transition in Diffuse-Type of Gastric Cancer. *Cancers* **2020**, *12*, 2741. [[CrossRef](#)]
3. Perrot-Appinat, M.; Vacher, S.; Pimpie, C.; Chemlali, W.; Derieux, S.; Pocard, M.; Bieche, I. Differential gene expression in growth factors, epithelial mesenchymal transition and chemotaxis in the diffuse type compared with the intestinal type of gastric cancer. *Oncol. Lett.* **2019**, *18*, 674–686. [[CrossRef](#)]
4. Tanabe, S.; Quader, S.; Cabral, H.; Ono, R. Interplay of EMT and CSC in Cancer and the Potential Therapeutic Strategies. *Front. Pharmacol.* **2020**, *11*, 904. [[CrossRef](#)]
5. Lambert, A.W.; Pattabiraman, D.R.; Weinberg, R.A. Emerging Biological Principles of Metastasis. *Cell* **2017**, *168*, 670–691. [[CrossRef](#)]
6. Du, B.; Shim, J.S. Targeting Epithelial-Mesenchymal Transition (EMT) to Overcome Drug Resistance in Cancer. *Molecules* **2016**, *21*, 965. [[CrossRef](#)]
7. Zhang, Y.; Weinberg, R.A. Epithelial-to-mesenchymal transition in cancer: Complexity and opportunities. *Front. Med.* **2018**, *12*, 361–373. [[CrossRef](#)]
8. Sommers, C.L.; Heckford, S.E.; Skerker, J.M.; Worland, P.; Torri, J.A.; Thompson, E.W.; Byers, S.W.; Gelmann, E.P. Loss of epithelial markers and acquisition of vimentin expression in adriamycin- and vinblastine-resistant human breast cancer cell lines. *Cancer Res.* **1992**, *52*, 5190–5197.
9. Kaimori, A.; Potter, J.; Kaimori, J.Y.; Wang, C.; Mezey, E.; Koteish, A. Transforming growth factor-beta1 induces an epithelial-to-mesenchymal transition state in mouse hepatocytes in vitro. *J. Biol. Chem.* **2007**, *282*, 22089–22101. [[CrossRef](#)]
10. Yook, J.I.; Li, X.-Y.; Ota, I.; Fearon, E.R.; Weiss, S.J. Wnt-dependent Regulation of the E-cadherin Repressor Snail*. *J. Biol. Chem.* **2005**, *280*, 11740–11748. [[CrossRef](#)]
11. Babaei, G.; Aziz, S.G.; Jaghi, N.Z.Z. EMT, cancer stem cells and autophagy; The three main axes of metastasis. *Biomed Pharm.* **2021**, *133*, 110909. [[CrossRef](#)] [[PubMed](#)]
12. Hill, C.; Wang, Y. The importance of epithelial-mesenchymal transition and autophagy in cancer drug resistance. *Cancer Drug Resist.* **2020**, *3*, 38–47. [[CrossRef](#)] [[PubMed](#)]
13. Sanchez-Vega, F.; Mina, M.; Armenia, J.; Chatila, W.K.; Luna, A.; La, K.C.; Dimitriadou, S.; Liu, D.L.; Kantheti, H.S.; Sghafinia, S.; et al. Oncogenic Signaling Pathways in The Cancer Genome Atlas. *Cell* **2018**, *173*, 321–337.e310. [[CrossRef](#)] [[PubMed](#)]
14. Bass, A.J.; Thorsson, V.; Shmulevich, I.; Reynolds, S.M.; Miller, M.; Bernard, B.; Hinoue, T.; Laird, P.W.; Curtis, C.; Shen, H.; et al. Comprehensive molecular characterization of gastric adenocarcinoma. *Nature* **2014**, *513*, 202–209. [[CrossRef](#)]
15. Cerami, E.; Gao, J.; Dogrusoz, U.; Gross, B.E.; Sumer, S.O.; Aksoy, B.A.; Jacobsen, A.; Byrne, C.J.; Heuer, M.L.; Larsson, E.; et al. The cBio Cancer Genomics Portal: An Open Platform for Exploring Multidimensional Cancer Genomics Data. *Cancer Discov.* **2012**, *2*, 401–404. [[CrossRef](#)]
16. Gao, J.; Aksoy, B.A.; Dogrusoz, U.; Dresdner, G.; Gross, B.; Sumer, S.O.; Sun, Y.; Jacobsen, A.; Sinha, R.; Larsson, E.; et al. Integrative Analysis of Complex Cancer Genomics and Clinical Profiles Using the cBioPortal. *Sci. Signal.* **2013**, *6*, pl1. [[CrossRef](#)]

17. Grossman, R.L.; Heath, A.P.; Ferretti, V.; Varmus, H.E.; Lowy, D.R.; Kibbe, W.A.; Staudt, L.M. Toward a Shared Vision for Cancer Genomic Data. *N. Engl. J. Med.* **2016**, *375*, 1109–1112. [[CrossRef](#)]
18. Tanabe, S.; Quader, S.; Ono, R.; Cabral, H.; Aoyagi, K.; Hirose, A.; Yokozaki, H.; Sasaki, H. Cell Cycle Regulation and DNA Damage Response Networks in Diffuse- and Intestinal-Type Gastric Cancer. *Cancers* **2021**, *13*, 5786. [[CrossRef](#)]
19. Krämer, A.; Green, J.; Pollard, J., Jr.; Tugendreich, S. Causal analysis approaches in Ingenuity Pathway Analysis. *Bioinformatics* **2013**, *30*, 523–530. [[CrossRef](#)]
20. Pospisil, P.; Iyer, L.K.; Adelstein, S.J.; Kassis, A.I. A combined approach to data mining of textual and structured data to identify cancer-related targets. *BMC Bioinform.* **2006**, *7*, 354. [[CrossRef](#)]
21. Breiman, L. Random Forests. *Mach. Learn.* **2001**, *45*, 5–32. [[CrossRef](#)]
22. Friedman, J.H. Greedy function approximation: A gradient boosting machine. *Ann. Stat.* **2001**, *29*, 1189–1232. [[CrossRef](#)]
23. Liu, D.; Wang, X.; Li, L.; Jiang, Q.; Li, X.; Liu, M.; Wang, W.; Shi, E.; Zhang, C.; Wang, Y.; et al. Machine Learning-Based Model for the Prognosis of Postoperative Gastric Cancer. *Cancer Manag. Res.* **2022**, *14*, 135–155. [[CrossRef](#)]
24. Scavo, M.P.; Fucci, L.; Caldarola, L.; Mangia, A.; Azzariti, A.; Simone, G.; Gasparini, G.; Krol, S. Frizzled-10 and cancer progression: Is it a new prognostic marker? *Oncotarget* **2018**, *9*, 824–830. [[CrossRef](#)]
25. Cheng, Y.; Li, L.; Pan, S.; Jiang, H.; Jin, H. Targeting Frizzled-7 Decreases Stemness and Chemotherapeutic Resistance in Gastric Cancer Cells by Suppressing Myc Expression. *Med. Sci. Monit.* **2019**, *25*, 8637–8644. [[CrossRef](#)]
26. Nusse, R.; Clevers, H. Wnt/ β -Catenin Signaling, Disease, and Emerging Therapeutic Modalities. *Cell* **2017**, *169*, 985–999. [[CrossRef](#)]
27. Peng, Y.; Zhang, X.; Lin, H.; Deng, S.; Qin, Y.; Yuan, Y.; Feng, X.; Wang, J.; Chen, W.; Hu, F.; et al. SUFU mediates EMT and Wnt/ β -catenin signaling pathway activation promoted by miRNA-324-5p in human gastric cancer. *Cell Cycle* **2020**, *19*, 2720–2733. [[CrossRef](#)]
28. Chi, Y.; Wang, F.; Zhang, T.; Xu, H.; Zhang, Y.; Shan, Z.; Wu, S.; Fan, Q.; Sun, Y. miR-516a-3p inhibits breast cancer cell growth and EMT by blocking the Pygo2/Wnt signalling pathway. *J. Cell Mol. Med.* **2019**, *23*, 6295–6307. [[CrossRef](#)]
29. Wang, Z.X.; Chen, Y.Y.; Li, B.A.; Tan, G.W.; Liu, X.Y.; Shen, S.H.; Zhu, H.W.; Wang, H.D. Decreased pygopus 2 expression suppresses glioblastoma U251 cell growth. *J. Neurooncol.* **2010**, *100*, 31–41. [[CrossRef](#)]
30. Zhang, D.; Liu, Y.; Wu, Q.; Zheng, Y.; Kaweme, N.M.; Zhang, Z.; Cai, M.; Dong, Y. Pygo2 as a novel biomarker in gastric cancer for monitoring drug resistance by upregulating MDR1. *J. Cancer* **2021**, *12*, 2952–2959. [[CrossRef](#)]
31. Ye, C.; Ho, D.J.; Neri, M.; Yang, C.; Kulkarni, T.; Randhawa, R.; Henault, M.; Mostacci, N.; Farmer, P.; Renner, S.; et al. DRUG-seq for miniaturized high-throughput transcriptome profiling in drug discovery. *Nat. Commun.* **2018**, *9*, 4307. [[CrossRef](#)] [[PubMed](#)]
32. Hammerich-Hille, S.; Kaiparettu, B.A.; Tsimelzon, A.; Creighton, C.J.; Jiang, S.; Polo, J.M.; Melnick, A.; Meyer, R.; Oesterreich, S. SAFB1 mediates repression of immune regulators and apoptotic genes in breast cancer cells. *J. Biol. Chem.* **2010**, *285*, 3608–3616. [[CrossRef](#)] [[PubMed](#)]
33. Wyce, A.; Matteo, J.J.; Foley, S.W.; Felitsky, D.J.; Rajapurkar, S.R.; Zhang, X.P.; Musso, M.C.; Korenchuk, S.; Karpinich, N.O.; Keenan, K.M.; et al. MEK inhibitors overcome resistance to BET inhibition across a number of solid and hematologic cancers. *Oncogenesis* **2018**, *7*, 35. [[CrossRef](#)] [[PubMed](#)]
34. Tanabe, S.; Perkins, E.J.; Ono, R.; Sasaki, H. Artificial intelligence in gastrointestinal diseases. *Artif. Intell. Gastroenterol.* **2021**, *2*, 69–76. [[CrossRef](#)]
35. Gonzalez, D.M.; Medici, D. Signaling mechanisms of the epithelial-mesenchymal transition. *Sci. Signal.* **2014**, *7*, re8. [[CrossRef](#)]

Disclaimer/Publisher’s Note: The statements, opinions and data contained in all publications are solely those of the individual author(s) and contributor(s) and not of MDPI and/or the editor(s). MDPI and/or the editor(s) disclaim responsibility for any injury to people or property resulting from any ideas, methods, instructions or products referred to in the content.